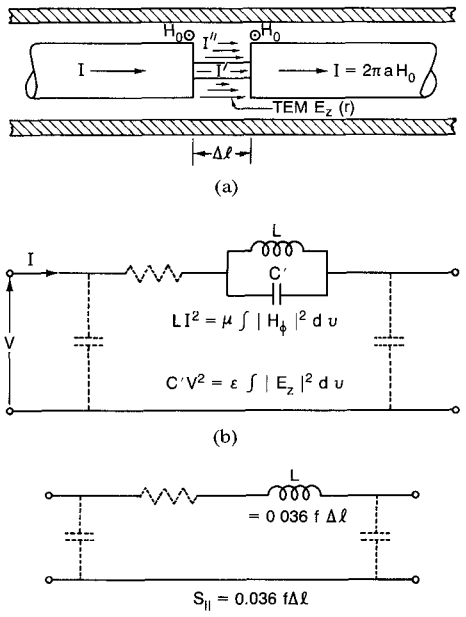

Fig. 4. (a) A close look at the fields and currents in the gap of joint J1. (b) An equivalent circuit for (a). (c) The inductance L and reflection coefficient S_{11} for J1.

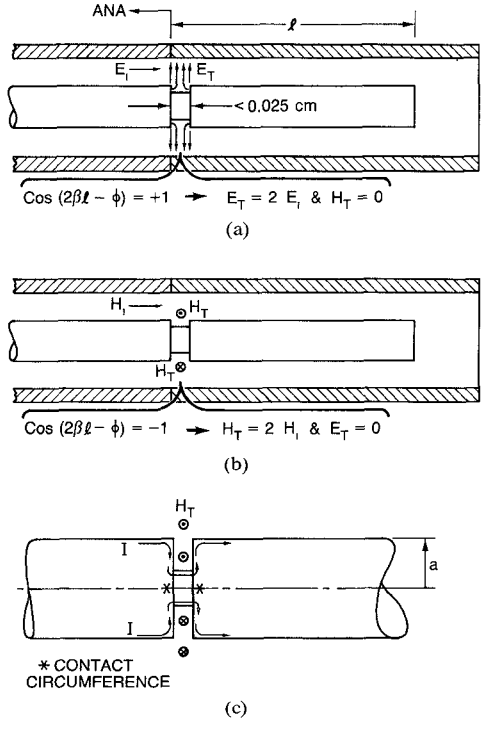

Fig. 5. (a) Longitudinal view of the line and open circuit where the frequency is such that the total electric field at the gap is a maximum and the magnetic field vanishes. (b) Longitudinal view where the frequency is such that the total magnetic field at the gap is a maximum and the electric field vanishes. (c) A closer view of the gap.

E_i, and the magnetic field vanishes. The gap is so narrow that no higher order modes penetrate it to reach the bottom of the gap, but their presence in the vicinity of the gap causes the fringing field shown in Fig. 1(b) and results in the discontinuity capacitances (last term in (8)). There is no current to penetrate the gap, so the gap resistance causes no voltage drop and goes unnoticed.

When the frequency is such that $\cos(2\beta l + \phi)$ is equal to -1, the total magnetic field is twice the incident field, and the electric field vanishes (Fig. 5(b)). Now there are no electric field lines at all and the discontinuity capacitances are unexcited. However, the circulating magnetic field H_T (Fig. 5(c)) causes a current that samples the gap resistance r (last term in (7)). The current encounters the two contact resistances at the bottom of the gap that represent the metal-to-metal contacts in the actual connector joint. Current flowing across these contacts causes a significant loss, which is reflected in the normalized resistance r. The distributed or skin loss on the sides of the gap can also be included in r, although it is not significant compared to the contact loss.

ACKNOWLEDGMENT

The author is greatly indebted to four colleagues in the Electromagnetic Fields Division of the National Bureau of Standards: G. J. Counas, R. L. Ehret, J. R. Juroshek, and B. C. Yates.

REFERENCES

[1] W. C. Daywitt, "A simple technique for determining joint losses on a coaxial line from swept-frequency reflection data," (to be published in) Proc. IEEE CPEM'86 Conf., Gaithersburg, MD, June 1986.
[2] J. D. Jackson, *Classical Electrodynamics*. New York: Wiley, 1962.
[3] J. R Whinnery, H. W. Jamieson, and T E. Robbins, "Coaxial-line discontinuities," *Proc. IRE*, p. 695, Nov. 1944.
[4] D. M. Kerns and R. W Beatty, *Basic Theory of Waveguide Junctions and Introductory Microwave Network Analysis* New York: Pergamon Press. 1967.
[5] J. R Juroshek, "A study of measurements of connector repeatibility using highly reflecting loads," pp. 457–460, this issue.
[6] N. Marcuvitz, ed., *Waveguide Handbook* New York: McGraw-Hill, 1951.
[7] R. E Collin, *Foundations for Microwave Engineering*. New York: McGraw-Hill, 1966.

Analysis of Waveguiding Structures Employing Surface Magnetoplasmons by the Finite-Element Method

NADER MOHSENIAN, MEMBER, IEEE, TERRY J. DELPH, AND DONALD M. BOLLE, FELLOW, IEEE

***Abstract*—The dispersion relation and electromagnetic field distributions for a gyroelectrically loaded waveguiding structure are obtained utilizing finite-element techniques. The structure considered consists of two layers, one a dielectric and the other a semiconductor, bounded by two perfectly conducting planes. The finite-element solution for the lowest real branches in the dispersion spectrum was compared against a numerical solution of the exact dispersion equation, and excellent agreement was found between the two. The structure, exhibiting nonreciprocal behavior, provides a suitable canonical model for the design of circuit components such as circulators, isolators, and phase shifters.**

I. INTRODUCTION

The use of surface magnetoplasmons on semiconductor substrates shows promise in the development of components that can substitute for ferrite devices in the millimeter- and submillimeter-wave ranges [1]–[3]. Analytical studies of canonical struc-

Manuscript received August 18, 1986; revised November 28, 1986. This work was supported in part by the Army Research Office under Grant DAAG29-85-K-0081.

N. Mohsenian and D. M. Bolle are with the Department of Computer Science and Electrical Engineering, Lehigh University, Bethlehem, PA 18015.
T. J Delph is with the Department of Mechanical Engineering and Mechanics, Lehigh University, Bethlehem, PA 18015.

IEEE Log Number 8612947.

tures employing surface magnetoplasmons have been reported in [4]–[6]. As the geometry of gyroelectrically loaded waveguides becomes more complicated, the problem of obtaining the dispersive behavior and the distribution of field intensities in the structure demands more sophisticated techniques. One particularly attractive means of dealing with this problem is the finite-element technique. This method has been successfully applied to microwave and optical waveguides, e.g., [7]. In this paper, we present a finite-element formulation for TM-mode wave propagation in a dielectric–semiconductor waveguide.

II. The Waveguiding Structure

We consider the two-layer dielectric–semiconductor structure, sided by two perfectly conducting planes, shown in the insert of Fig. 1. A finite-element mesh is shown superposed. The thickness of the dielectric layer is taken to be P_1, while that of the semiconduting layer is P_2. The substrate for the semiconductor region is assumed to be a high-quality, moderately doped n-type GaAs material with a carrier concentration of $n \simeq 2.1\times10^{15}$ cm^{-3}, equivalent to a plasma frequency of $\omega_p = 10^{13}$ rad/s. The permeability μ is taken to be a constant for both regions. A uniform dc magnetic field corresponding to a cyclotron frequency $\omega_c = 10^{12}$ rad/s ($B_0 = 3810$ G) is assumed to be applied parallel to the interface. For a biasing magnetic field in the y direction, the permittivity ϵ remains a constant for the dielectric medium, but becomes an asymmetric tensor for the semiconducting medium, [4]–[6], having the form

$$\epsilon_2(\omega) = \begin{bmatrix} \xi & 0 & -j\eta \\ 0 & \zeta & 0 \\ j\eta & 0 & \xi \end{bmatrix} \tag{1}$$

where

$$\xi = \epsilon^{(0)} - \frac{\omega_p^2(\omega - j\nu)}{\omega\left[(\omega - j\nu)^2 - \omega_c^2\right]} \quad \zeta = \epsilon^{(0)} - \frac{\omega_p^2}{\omega(\omega - j\nu)}$$

$$\eta = \frac{-\omega_p^2\omega_c}{\omega\left[(\omega - j\nu)^2 - \omega_c^2\right]}.$$

Here, $\epsilon^{(0)}$ is the static dielectric constant of the semiconducting medium, ω is the frequency of electromagnetic wave propagation, and ν is the collision frequency. Finally, the semiconductor and dielectric here are taken to be lossless, implying $\nu = 0$.

In the present analysis, we will consider only TM wave modes, because TE modes do not exhibit interesting interactions with the semiconducting material. This implies that only the h_y, e_x, and e_z field components are nonvanishing. We now assume time-harmonic wave propagation in the z direction with frequency ω and propagation constant $\gamma = \alpha + j\beta$, so that $e_z = e_z(x, y)e^{j\omega t - \gamma z}$. With these assumptions, an uncoupled partial differential equation may be derived for e_z from Maxwell's equations. This equation has the general form

$$\frac{\partial^2 e_z}{\partial x^2} + M_1\frac{\partial^2 e_z}{\partial y^2} + M_2 e_z = 0 \tag{2}$$

where for the semiconducting medium

$$M_1 = \frac{\zeta\left(\gamma^2 + \omega^2\mu_0\epsilon_0\xi\right)}{\xi\left(\gamma^2 + \omega^2\mu_0\epsilon_0\zeta\right)} \quad M_2 = \gamma^2 + \frac{\omega^2\mu_0\epsilon_0\left(\xi^2 - \eta^2\right)}{\xi}$$

and for the dielectric medium

$$M_1 = 1 \quad M_2 = \gamma^2 + \omega^2\mu_0\epsilon_0\epsilon_1.$$

Here, ϵ_0 and μ_0 are the vacuum permittivity and permeability, and ϵ_1 is the relative dielectric constant of the dielectric medium.

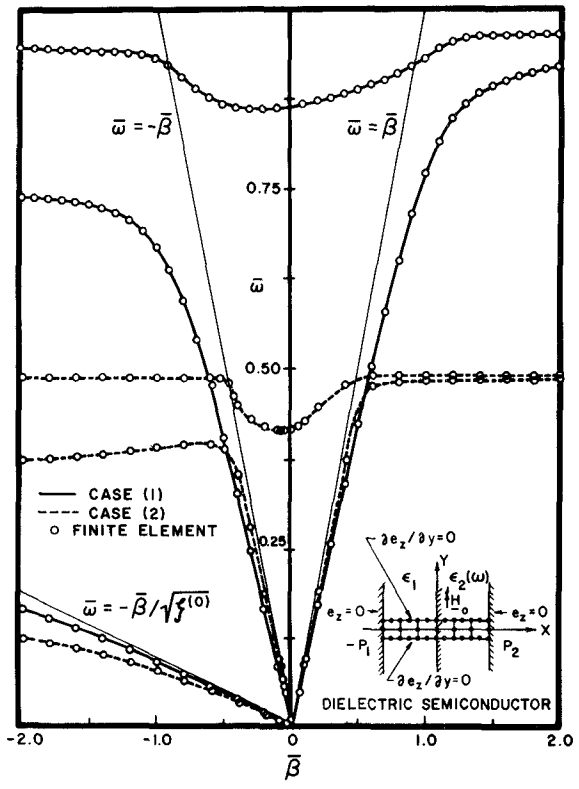

Fig. 1. Exact and finite-element dispersion spectra of a dielectric–semiconductor single interface for case (1): $P_1 = 80$ μm, $P_2 = 100$ μm and case (2): $P_1 = 320$ μm, $P_2 = 50$ μm.

The waveguiding structure shown in Fig. 1 is, of course, strictly one-dimensional, so that $\partial()/\partial y = 0$. Solving Maxwell's equations and applying the boundary conditions at the planes and at the interface, we obtain the dispersion equation, which is

$$\left(\frac{\epsilon_1}{k_1}\right)\coth(k_1P_1) = \left(\frac{\xi k_2}{\gamma^2 + \omega^2\mu_0\epsilon_0\xi}\right) \cdot \coth(k_2P_2) - \left(\frac{j\eta\gamma}{\gamma^2 + \omega^2\mu_0\epsilon_0\xi}\right) \tag{3}$$

where

$$k_1^2 = -\gamma^2 - k_0^2\epsilon_1 \quad k_2^2 = -\gamma^2 - k_0^2\epsilon_e(\omega) \quad k_0^2 = \omega^2\mu_0\epsilon_0$$

$$\epsilon_e(\omega) = \frac{\xi^2 - \eta^2}{\xi}.$$

III. Finite-Element Formulation

Because the governing equation (2) for the e_z field component is uncoupled and because the other field components are easily expressible in terms of e_z through Maxwell's equations, e_z was chosen as the dependent variable for the finite-element formulation. For the sake of generality, the finite-element equations will be derived in two-dimensional terms using (2), even though the problem to be treated is strictly one-dimensional. In the present case, the finite-element equations are most conveniently generated by means of the Galerkin formulation. This yields

$$\iint_A \left(\frac{\partial^2 e_z}{\partial x^2} + M_1\frac{\partial^2 e_z}{\partial y^2} + M_2 e_z\right) N_i(x, y)\, dx\, dy = 0 \tag{4}$$

where the $N_i(x, y)$ are the finite-element interpolating (shape) functions for the problem, and the index i ranges over those

nodal points at which no geometric boundary conditions are imposed for e_z. The interpolating functions are used to approximate $e_z(x, y)$ in the following manner: $e_z(x, y) \simeq [N(x, y)]\{e_z\}$, where $[N(x, y)]$ is the row vector of interpolating functions and $\{e_z\}$ is the column vector of nodal point values. An application of the divergence theorem now yields the finite-element equations in the form

$$[T]\{e_z\} - \oint_{\bar{B}} \left(\frac{\partial e_z}{\partial x} n_x + M_1 \frac{\partial e_z}{\partial y} n_y \right) N_i \, ds = 0. \tag{5}$$

The i, jth element in the coefficient matrix $[T]$ is given by

$$T_{ij} = \int\int_A \left(\frac{\partial N_i}{\partial x} \frac{\partial N_j}{\partial x} + M_1 \frac{\partial N_i}{\partial y} \frac{\partial N_j}{\partial y} - M_2 N_i N_j \right) dx\, dy. \tag{6}$$

The line integral in (5) is to be evaluated around the boundary $\bar{B}$ of the area A under consideration, with (n_x, n_y) being the components of the unit normal vector to $\bar{B}$. The finite-element equations are assembled from the element contributions to (5), the boundary integral being evaluated around the boundary $\bar{B}_e$ of each element. It is not difficult to show that the line integral vanishes everywhere except along the interface between the dielectric and semiconducting regions, where special care must be taken. Let n be one of the values of the index i corresponding to the interface nodes. Further, denote the values of e_z in the dielectric and semiconducting regions of $e_z^{(1)}$ and $e_z^{(2)}$, respectively. Along the interface, we must have both continuity of e_z, $e_z^{(1)} = e_z^{(2)}$, and continuity of h_y. The latter condition, from Maxwell's equations, gives

$$\left. \frac{\partial e_z^{(1)}}{\partial x} \right|_{x=0} = \left. \left(R_1 \frac{\partial e_z^{(2)}}{\partial x} + R_2 e_z^{(2)} \right) \right|_{x=0} = C \tag{7}$$

where

$$R_1 = \frac{\xi\left(\gamma^2 + \omega^2 \mu_0 \epsilon_0 \epsilon_1\right)}{\epsilon_1\left(\gamma^2 + \omega^2 \mu_0 \epsilon_0 \xi\right)} \qquad R_2 = \left(\frac{j\eta\gamma}{\xi} \right) R_1.$$

We now write the nth finite-element equation separately for both the dielectric and the semiconducting region. Taking account of the fact that $n_x = \pm 1, n_y = 0$ along the interface, and making use of (7), we have, respectively (with summation convention for repeated subscripts implied),

$$T_{nj}^{(1)} e_{zj}^{(1)} = C d_n \tag{8}$$

$$T_{nj}^{(2)} e_{zj}^{(2)} - \left(\frac{R_2}{R_1} \right) b_{nj} e_{zj}^{(2)} = \frac{C d_n}{R_1} \tag{9}$$

where

$$d_n = \int_{-\delta}^{\delta} N_n(0, y)\, dy \qquad b_{nj} = \int_{-\delta}^{\delta} N_n(0, y) N_j(0, y)\, dy.$$

Here δ and $-\delta$ represent the y coordinates of the nodes on the top and bottom of the elements, taken to be $\delta = 15\ \mu$m. Eliminating C between (8) and (9) and requiring continuity of e_z at the interface, $e_{zn}^{(1)} = e_{zn}^{(2)}$, now yields for the nth equation

$$\left(T_{nj}^{(1)} + R_1 T_{nj}^{(2)} - R_2 b_{nj} \right) e_{zj} = 0. \tag{10}$$

Equation (10) represents the finite-element equations corresponding to the interface nodes. The remaining finite-element equations have the form of (5), with the line integral vanishing for these equations. It is worth noting that the inclusion of the terms with coefficients R_1 and R_2 in (10) renders the resulting finite-element coefficient matrix $[T^*]$ nonsymmetric, even though the basic coefficient matrix $[T]$ in (5) is symmetric. When assembled, the finite-element equations have the form $[T^*]\{e_z\} = 0$. A nontrivial solution then requires that

$$|T^*| = 0. \tag{11}$$

Equation (11) represents the finite-element dispersion equation for the problem. Given a value of ω, one may obtain corresponding values of γ by evaluating $|T^*|$ numerically and employing standard numerical root-finding techniques.

IV. Results

Numerical results for the dispersion spectrum, using a numerical root-finding technique, were obtained from both the exact dispersion relation given by (3) and the approximate finite-element formulation given by (11). Two different combinations of layer thicknesses were considered. In case (1), $P_1 = 80\ \mu$m and $P_2 = 100\ \mu$m, and in case (2), $P_1 = 320\ \mu$m and $P_2 = 50\ \mu$m. Furthermore, it was assumed that $\epsilon_1 = 1, \epsilon^{(0)} = 13$. For the finite-element analysis, the two layers were divided into three equisized elements (Fig. 1) using eight-noded isoparametric quadrilateral elements. Fig. 1 shows the resulting dispersion spectra for both combinations of thicknesses in terms of a normalized propagation constant defined by $\bar{\beta} = P_2 \beta$ and a normalized frequency given by $\bar{\omega} = \omega P_2 / c$, where c is the velocity of light. Nonreciprocal effects are evident in both branches of the spectrum. It can be seen that excellent agreement exists between the spectra computed from the exact dispersion relation and the approximate finite-element result.

At low frequencies, a reverse-propagating mode was obtained in both cases, with the bulk of its energy traveling in the semiconducting medium. For small values of $\bar{\omega}$, this branch becomes asymptotic to the light line of the semiconducting medium; i.e., $\bar{\omega} \to -\bar{\beta}/\sqrt{\xi^{(0)}}$ as $\bar{\omega} \to 0$, where $\xi^{(0)}$ is defined by: $\xi^{(0)} = \epsilon^{(0)} + (\omega_p/\omega_c)^2$. The absence of a forward-propagating mode over this frequency range may be explained through examining the configuration of the field distributions shown in Fig. 2(a). If such a mode existed, most of its energy would need to be concentrated in the semiconducting medium and to be traveling in the positive z direction. The field components of the dielectric medium would display the same behavior as those derived for the reverse mode. To justify the direction of the signal, the e_x component should exhibit a negative amplitude in the semiconducting medium. But for the given electrical parameters of this problem, the tensor elements ξ and η yield positive values and these conditions do not allow the fulfilling of the continuity of the normal component of the $\boldsymbol{D}$ field. Consequently, there exists only a unidirectional mode, which propagates in the reverse direction over this frequency range, i.e., $\bar{\omega} < 0.17$. When losses are introduced, this mode will suffer substantial attenuation; therefore, the remaining branches of the spectrum are the ones of primary interest.

In both cases, the lower branches of the forward and reverse propagation modes become asymptotic to the light line, i.e., $\bar{\omega} \to \pm\bar{\beta}$ as $\bar{\omega} \to 0$. However, for higher frequencies, the forward mode extends into a region where the quantity k_2^2 becomes negative. In this region, the transverse field components have a trigonometric variation in the semiconducting medium. The upper branches lie entirely in this region, and are called the "volume" modes [5], [6].

Also observed in case (2) is a change of slope in the lower branch of the reverse-propagating mode. This may be understood through the field displacement behavior of the mode in the structure. Here, unlike case (1), the transverse component of the magnetic field clings to the plane at $x = P_2$ for $\bar{\beta} < -0.6$, as

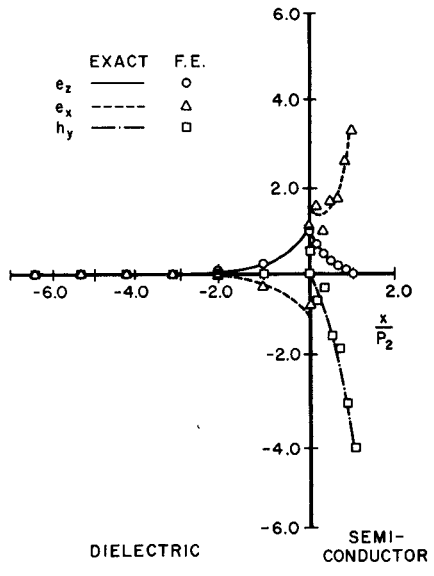

(a)

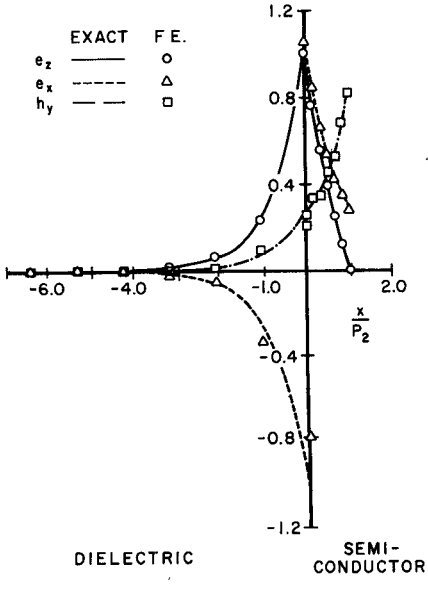

(b)

Fig. 2. Model field distributions of components (e_z, e_x, h_y) taken from the branches of the exact and finite-element (F.E.) dispersion spectra for case (2): $P_1 = 320\ \mu$m, $P_2 = 50\ \mu$m. (a) Unidirectional branch, $\bar{\beta} = -1.4$, $\bar{\omega} = .101$. (b) Lower branch, $\bar{\beta} = -1.4$, $\bar{\omega} = .381$.

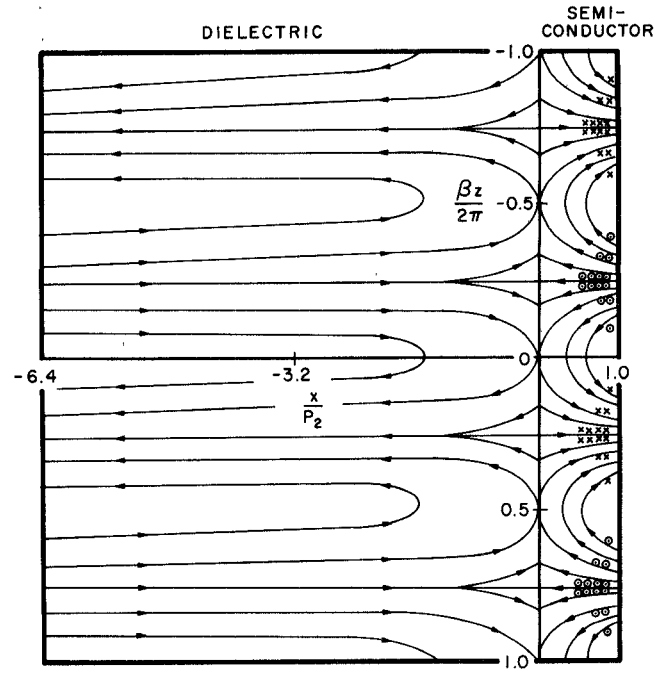

(a)

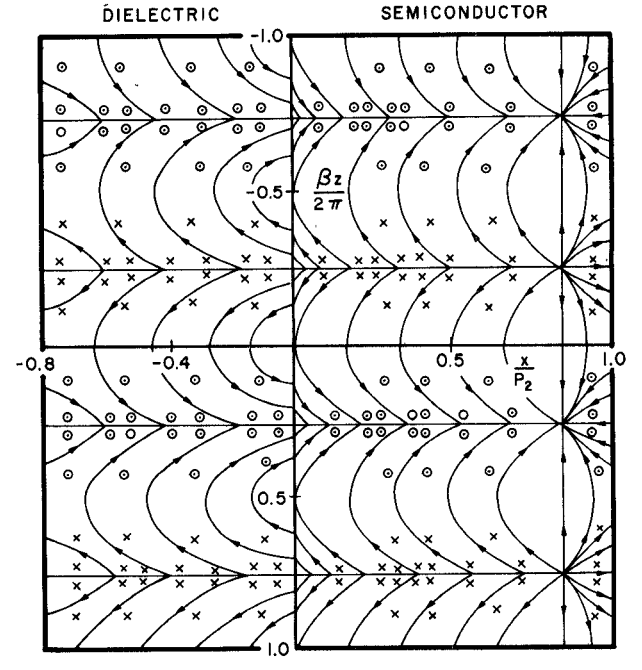

(b)

Fig. 3. Field structure of components E(——) and H(⊙, ×) obtained from the finite-element formulation for case (1): $P_1 = 80\ \mu$m, $P_2 = 100\ \mu$m and case (2): $P_1 = 320\ \mu$m, $P_2 = 50\ \mu$m. (a) Case (2), unidirectional branch, $\bar{\beta} = -1.0$, $\bar{\omega} = .078$. (b) Case (1), lower branch, $\bar{\beta} = 1.2$, $\bar{\omega} = .847$.

shown in Fig. 2(b). For this portion of the branch, the direction of the energy flow is reversed, and with the energy traveling in the positive direction, a change in the slope of the branch is obtained.

Of interest is the fact that there exists a frequency band above the lower reverse mode which contains only a forward mode. This offers the possibility of designing components such as isolators and circulators having a small attenuation constant when losses and a more realistic geometry are considered. For the particular set of geometric and electrical parameters used here, this frequency band was calculated to be 358 GHz $< f <$ 411 GHz for case (1) and 377 GHz $< f <$ 396 GHz for case (2), with the former case having a 15-percent bandwidth.

Fig. 2 shows the modal field distributions for the components (e_z, e_x, h_y) derived from both the exact and finite-element (F.E.) solutions. Here, for comparison purposes only, the h_y component was normalized by the factor η_0 for the lower branch and by the factor $\eta_0/10$ for the unidirectional branch, where $\eta_0 = 376.82\ \Omega$ is the impedance of free space. The value of e_z at the interface is normalized to unity. For the linear region of the lower branches in both cases, most of the energy is seen to be contained within the dielectric medium, while the energy is essentially uniformly distributed throughout the structure as these branches move away from the light line. The upper branches in case (1) also exhibit similar energy distribution, but the behavior of case (2) is some-

what different. Here, the bulk of the energy shifts to the semiconducting medium, while at the very low end of the upper branches a fairly uniform distribution of energy may be noted. Finally, the field structures of the components (e_z, e_x, h_y) derived from the finite-element formulation are shown in Fig. 3 at time $t = 0$. These patterns do not attempt to show the relative field strengths, but only the directions. However, the relative field strengths between the two media can be observed in the previous figure.

V. Conclusions

A numerical analysis based on the finite-element formulation has been presented for a canonical, one-dimensional, gyroelectrically loaded waveguiding structure. The agreement between the finite-element solution and that obtained from the exact dispersion equation can be seen to be excellent and was, in fact, good to three significant figures. The primary advantage of the finite-element method is, of course, its ability to treat problems of practical interest involving complicated two-dimensional geometries and correspondingly complicated electric and magnetic field distributions. The results given here indicate that the finite-element method holds substantial promise for such applications, and gives the necessary confidence for its use in the analysis of electromagnetic wave propagation in much more complex gyroelectrically and gyromagnetically loaded waveguiding structures, where exact methods of analysis are not available.

References

[1] R. E. Hayes and W. G. May, "The use of semiconductors in nonreciprocal devices for submillimeter wavelengths," in *Proc. Symp. Submillimeter Waves* (Polytechnic Inst. Brooklyn), 1970, pp. 237–250.

[2] M. Kanda and W. G. May, "Hollow-cylinder waveguide isolators for use at millimeter wavelengths," *IEEE Trans. Microwave Theory Tech.*, vol. MTT-22, pp. 913–917, Nov. 1974.

[3] M. Kanda and W. G. May, "A millimeter-wave reflection-beam isolator," *IEEE Trans. Microwave Theory Tech.*, vol. MTT-23, pp. 506–508, June 1975.

[4] W. L. K. Hwang, "Application of surface magnetoplasmons on semiconductor substrates," Ph.D thesis, Dept Computer Sci. & Elec Eng., Lehigh University, Bethlehem, PA, 1983.

[5] S H. Talisa and D. M. Bolle, "Fundamental considerations in millimeter and near-millimeter component design employing magnetoplasmons," *IEEE Trans. Microwave Theory Tech.*, vol. MTT-29, pp. 916–923, Sept 1981.

[6] S. H. Talisa and D. M. Bolle, "Performance predictions for isolators and differential phase shifters for the near-millimeter wave ranges," *IEEE Trans. Microwave Theory Tech.*, vol. MTT-29, pp. 1338–1343, Dec. 1981.

[7] B. M. A. Rahman and J. B. Davies, "Finite-element analysis of optical and microwave waveguide problems," *IEEE Trans. Microwave Theory Tech.*, vol. MTT-32, pp 20–28, Jan. 1984.